The spherical symmetry property of the compatible staggered Lagrangian scheme for elastic-plastic flows in two-dimensional cylindrical geometry

Li Liu,[1] Jun-bo Cheng [1,*], Zhanli Liu[2]

[1] *Institute of Applied Physics and Computational Mathematics, Beijing 100094, China*

[2] *Applied Mechanics Laboratory, Department of Engineering Mechanics, School of Aerospace, Tsinghua University, Beijing, China*

Abstract

A multi-material HLLC-type approximate Riemann solver with both elastic and plastic waves (MHLLCEP) is constructed for 1D elastic-plastic flows with the hypo-elastic model and the von Mises yielding condition. Although Cheng in 2016 [1] introduced a HLLC Riemann solver with elastic waves (HLLCE) for 1D elastic-plastic flows, Cheng assumed that pressure is continuous across a contact wave. This assumption may lead to numerical errors, especially for multi-material elastic-plastic flows. In our MHLLCEP, this assumption is not used again. Correspondingly, the errors introduced by the assumption are deleted, describing and evaluating the plastic waves are more accurate than that in the HLLCE. For the multi-material system, in this paper, a ghost cell method is used to eliminate the numerical oscillations and keep a high-order spatial reconstruction across the interface. Based on the MHLLCEP, combining with the third-order WENO reconstruction method and the third-order Runge-Kutta method in time, a high-order cell-centered Lagrangian scheme for 1D multi-material elastic-plastic flows is built in this paper. A number of numerical experiments are carried out. Numerical experiments show that the third-order scheme is robust, essentially non-oscillatory and, as suggested by numerical experiments,

*Correspondence to: Junbo Cheng, Institute of Applied Physics and Computational Mathematics, Beijing 100094, China. E-mail: Cheng_junbo@iapcm.ac.cn

may also be convergent. Moreover, for multi-material elastic-plastic flows, the scheme with the MHLLCEP is more accurate and reasonable in resolving the multi-material interface than the scheme with the HLLCE.
Keywords: HLLC Riemann solver, high-order cell-centered Lagrangian scheme, WENO scheme, hypo-elastic model, elastic-plastic flows

1. Introduction

In this paper, we give a detailed study of the spherical symmetric property of the compatible staggered Lagrangian scheme [], Including the usually used artificial viscosities [] and hourglass controlling methods [], for elastic-plastic flows in two-dimensional cylindrical coordinates with equal angular zoning. .

In areas of Inertial Confinement Fusion(ICF), cavitation and metal wilding, solids always undergoing high-velocity impacts, and need to be described as elastic-plastic flows, which was firstly introduced by Wilkins[]. In this paper, the model of elastic-plastic flow consists of the usual conservation laws of the mass, the momentum and the total energy and a hyperelastic-based constitutive law. There are mainly three ways to simulate the elastic-plastic flow, as Eulerian methods, cell-centered Lagrangian schemes and staggered Lagrangian schemes. Eulerian methods mainly use hyper-elastic models. Lagrangian schemes, including the cell-centered Lagrangian schemes and the staggered Lagrangian schemes, are mainly used in simulating the elastic-plastic flows, due to its distinguished advantage in capturing material interfaces. In the seminal paper of [], a staggered Lagrangian scheme is used, wherein, velocity is stored at vertices, while density and internal energy are stored at cell centers. This kind of Lagrangian schemes usually need artificial viscosities to ensure the entropy condition through shock waves and hourglass viscosities to deduce the zero energy modes.

Generally, elastic-plastic flows can be mainly simulated in three ways, Eulerian methods [4, 5, 6, 7], staggered Lagrangian schemes [3] and cell-centered Lagrangian schemes [8, 9, 10, 11] that are considered in this paper. Comparing

with the staggered Lagrangian scheme, the cell-centered Lagrangian schemes have many advantages. Firstly, it is not necessary to add extra artificial viscosity which must be used in the staggered Lagrangian schemes; secondly, it is easy to guarantee the total energy conservation; besides, it can also be used to simulate the problems with both hyper-elastic and hypo-elastic models [8, 9, 10, 11] as a Lagrangian scheme.

For a cell-centered Lagrangian scheme, a core process is to move the node of grids with the speed of fluids by solving a Riemann problem at each cell face. As the Riemann problem contains many physical structures, especially for elastic-plastic flows, such as elastic waves, plastic waves and contact waves , the property of the approximate Riemann solver is of great importance in the simulations. Recently, a lot of works have been done in this area. For example, Gavrilyuk et al. [12] analyzed the structure of the Riemann solution and constructed a Riemann solver for the linear elastic system of hyperbolic non-conservative models for transverse waves, wherein, an extra evolution equation was added in order to make the elastic transformations reversible in the absence of shock waves. Despres [13] built a shock solution to the non-conservative system of hypo-elasticity models and found that a sonic point is necessary to construct the compression solution that begins at a constrained compressed state. Cheng et al. [14] analyzed the wave structures of one-dimensional elastic-plastic flows and developed an effective two-rarefaction approximate Riemann solver with elastic waves (TRRSE) and built a second-order and a third-order cell-centered Lagrangian schemes based on the TRRSE, but the TRRSE is a little expensive as the iteration method is used. In [1], for one-dimensional elastic-plastic flows, Cheng introduced a HLLCE Riemann solver, which is fast and efficient in resolving elastic waves and plastic waves. In the HLLCE, Cheng evaluated the deviatoric stresses from the following *assumption: the pressure is continuous across the contact wave*. This assumption is valid for pure fluids, but in elastic-plastic flows, this assumption may lead to some errors. There are three cases we need to consider.

1. If states in the star regions on both sides of the contact wave are elastic, this assumption does not result in errors.
2. If both states reach the elastic limit, there are two cases that need to be taken into account:
   (a) if both materials on both sides of the interface are the same, this assumption does not result in errors either;
   (b) if materials are different, this assumption will result in big errors because the yielding strengths of different materials are always different.
3. If the state in one side of the interface reaches the elastic limit, but the state on another side is not, this assumption will also result in big errors.

In this paper, in order to eliminate these errors, we want to construct a new HLLC-type Riemann solver [15, 2] for 1D multi-material elastic-plastic flows. In the new solver, both the elastic waves and plastic waves are correctly resolved and the assumption in [1] that the pressure is continuous across the interface is deleted; correspondingly, the errors introduced by the assumption will also be eliminated.

Based on the MHLLCEP, we develop a high-order elastic-plastic cell-centered Lagrangian scheme for one-dimensional multi-material elastic-plastic flows. If we directly use the WENO reconstruction method [16, 17, 18] for multi-material elastic-plastic problems, the spacial stencil may cross the material interface and numerical oscillations may be caused near the interface. In order to delete the numerical oscillations near the material interface, a ghost cell method is used. Combined with an improved third-order WENO scheme[19] and the third-order Runge-Kutta scheme, a high-order cell-centered Lagrangian scheme is given in this paper for one-dimensional multi-material elastic-plastic flows.

This paper is organized as follows. In section 2, we briefly introduce the governing equations to be studied. In section 3, the MHLLCEP Riemann solver is constructed. Then, a high-order elastic-plastic cell-centered Lagrangian scheme is introduced in section 4. Some numerical examples are presented to validate the method in section 5. At last, conclusions are given.

2. Governing equations

In this paper, the elastic energy is not included in the total energy. The exclusion of the elastic energy is usual for practical engineering problems [10] and is different from that in Ref.[12].

2.1. Conservation equations

For the continuous one-dimensional solid, the conservation terms in differential form can be given as

$$\partial_t \mathbf{U} + \partial_x \boldsymbol{F}(\mathbf{U}) = 0,\ x \in\ \Omega \subset \mathbf{R},\ t > 0, \tag{1}$$

where

$$\mathbf{U} = \begin{bmatrix} \rho \\ \rho u \\ \rho E \end{bmatrix}, \quad \mathbf{F} = \begin{bmatrix} \rho u \\ \rho u^2 - \sigma_x \\ (\rho E - \sigma_x)u \end{bmatrix}, \tag{2}$$

ρ, u, σ_x and E are the density, the velocity in $x-$direction, the Cauchy stress and the total energy per unit volume, respectively, E has the relation with the specific internal energy e as

$$E = e + \frac{1}{2}u^2, \tag{3}$$

$$\sigma_x = -p + s_{xx}, \tag{4}$$

where p and s_{xx} denote the hydrostatic pressure and the deviatoric stress in the $x-$ direction, respectively.

2.2. The equation of state (EOS)

The relation of the pressure with the density and the specific internal energy is obtained from the equation of state (EOS). In this paper, we consider the Mie-Grüneisen EOS,

$$p(\rho, e) = \rho_0 a_0^2 f(\eta) + \rho_0 \Gamma_0 e, \tag{5}$$

where $f(\eta) = \frac{(\eta-1)(\eta-\Gamma_0(\eta-1)/2)}{(\eta-s(\eta-1))^2}$, $\eta = \frac{\rho}{\rho_0}$, ρ_0, a_0, s and Γ_0 are the constant parameters of the Mie-Grüneisen EOS.

2.3. The constitutive relation

Hooke's law is used here to describe the relationship between the deviatoric stress and the strain,

$$\dot{s}_{xx} = 2\mu \left(\dot{\varepsilon}_x - \frac{1}{3}\frac{\dot{V}}{V} \right), \tag{6}$$

where μ is the shear modulus, V is the volume, and the dot means the material time derivative,

$$\dot{()} = \frac{\partial()}{\partial t} + u\frac{\partial()}{\partial x}, \tag{7}$$

and

$$\dot{\varepsilon}_x = \frac{\partial u}{\partial x}, \quad \frac{\dot{V}}{V} = \frac{\partial u}{\partial x}. \tag{8}$$

By using Eq.(8), Eq.(6) can be rewritten as

$$\frac{\partial s_{xx}}{\partial t} + u\frac{\partial s_{xx}}{\partial x} = \frac{4}{3}\mu\frac{\partial u}{\partial x}. \tag{9}$$

2.4. The yielding condition

The Von Mises' yielding condition is used here to describe the elastic limit. In one spatial dimension, the von Mises' yielding criterion is given by

$$|s_{xx}| \leq \frac{2}{3}Y_0, \tag{10}$$

where Y_0 is the yield strength of the material in simple tension.

3. MHLLCEP approximate Riemann solver

3.1. The Riemann problem

The Riemann problem for the 1D time dependent elastic-plastic equations is given as follows:

$$\begin{cases} \partial_t \rho + \partial_x(\rho u) = 0, \\ \partial_t(\rho u) + \partial_x(\rho u^2 + p - s_{xx}) = 0, \\ \partial_t(\rho E) + \partial_x\left[(\rho E + p - s_{xx})u\right] = 0, \\ \partial_t s_{xx} + u\partial_x s_{xx} - \dfrac{4\mu}{3}\partial_x u = 0, \\ |s_{xx}| \le \dfrac{2}{3}Y_0, \\ Q(x, t=0) = \begin{cases} Q_L, \text{ if } x < 0, \\ Q_R, \text{ if } x > 0, \end{cases} \end{cases} \tag{11}$$

where $Q = (\rho, \rho u, \rho E, s_{xx})^T$.

3.2. Jacobian matrix

For the Mie-Grüneisen EOS, the system (11) can be written as

$$\partial_t \mathbf{Q} + \mathbf{J}(\mathbf{Q})\partial_x \mathbf{Q} = 0, \tag{12}$$

where

$$J = \begin{bmatrix} 0 & 1 & 0 & 0 \\ -u^2 + \frac{\partial p}{\partial \rho} + \Gamma(\frac{u^2}{2} - e) & u(2-\Gamma) & \Gamma & -1 \\ (\Gamma(\frac{u^2}{2} - e) - e + \frac{\sigma_x}{\rho} + \frac{\partial p}{\partial \rho})u & -\Gamma u^2 - \frac{\sigma_x}{\rho} + e & (1+\Gamma)u & -u \\ \frac{4}{3}\mu\frac{u}{\rho} & -\frac{4}{3}\mu\frac{1}{\rho} & 0 & u \end{bmatrix}, \tag{13}$$

where $\Gamma = \frac{\Gamma_0 \rho_0}{\rho}$.

The eigenvalues of the coefficient matrix $\mathbf{J}(\mathbf{Q})$ are given as

$$\lambda_1 = u - c, \quad \lambda_2 = \lambda_3 = u, \quad \lambda_4 = u + c, \tag{14}$$

where

$$\begin{cases} c = \sqrt{a^2 - \dfrac{\rho_0}{\rho^2}\Gamma_0 s_{xx} + \dfrac{4}{3}\dfrac{\mu}{\rho}}, \\ a^2 = \dfrac{\partial p}{\partial \rho} + \dfrac{p}{\rho^2}\dfrac{\partial p}{\partial e} = a_0^2 \dfrac{\partial f}{\partial \eta} + \dfrac{p}{\rho^2}\rho_0\Gamma_0. \end{cases} \tag{15}$$

The corresponding right eigenvectors are

$$r_1 = \frac{1}{\phi^2}\begin{bmatrix} 1 \\ u-c \\ h-uc \\ \phi^2 \end{bmatrix}, \quad r_2 = \begin{bmatrix} \frac{1}{b_1} \\ \frac{u}{b_1} \\ 0 \\ 1 \end{bmatrix}, \quad r_3 = \begin{bmatrix} -\frac{\Gamma}{b_1} \\ -\frac{\Gamma u}{b_1} \\ 1 \\ 0 \end{bmatrix}, \quad r_4 = \frac{1}{\phi^2}\begin{bmatrix} 1 \\ u+c \\ h+uc \\ \phi^2 \end{bmatrix}, \tag{16}$$

where

$$b_1 = \frac{\partial p}{\partial \rho} - \Gamma E, \quad h = E + \frac{p - s_{xx}}{\rho}, \tag{17}$$

and

$$\phi^2 = a^2 - \frac{\rho_0}{\rho^2}\Gamma_0 s_{xx} - c^2 = -\frac{4\mu}{3}\frac{1}{\rho}. \tag{18}$$

3.3. Formulations across the contact wave

For a system without molecular diffusion, there are no materials convecting across the contact wave or interface, so the velocities on two sides of the discontinuity are always equal. This can also be verified by the eigenvectors in Eq.(16).

Use $\mathbf{W}_L^*$ and $\mathbf{W}_R^*$ to denote the two states connected by the contact wave in the solution, where $\mathbf{W} = (\rho, u, p, s_{xx})$.

Thanks to Eq.(16), for the λ_2-wave we have

$$\frac{d\rho}{\frac{1}{b_1}} = \frac{d\rho u}{\frac{u}{b_1}} = \frac{d\rho E}{0} = \frac{ds_{xx}}{1}. \tag{19}$$

From the above equations, we can easily deduce that

$$du = 0, \quad d(s_{xx} - p) = 0, \tag{20}$$

which means

$$u_L^* = u_R^*, \tag{21}$$

and

$$\sigma_{x,L}^* = \sigma_{x,R}^*, \tag{22}$$

where $()_L^*$ and $()_R^*$ denote $()$ in the region of $\mathbf{W}_L^*$ and $\mathbf{W}_R^*$, respectively. Here we do not show the details of the derivation for a simple presentation.

Similarly, for the λ_3-wave one has

$$\frac{d\rho}{\frac{-\Gamma}{b_1}} = \frac{d\rho u}{\frac{-u\Gamma}{b_1}} = \frac{d\rho E}{1} = \frac{ds_{xx}}{0}. \tag{23}$$

From the above equations, we can easily deduce that

$$du = 0, \quad dp = 0, \quad ds_{xx} = 0, \tag{24}$$

which means

$$u_L^* = u_R^*, \tag{25}$$

$$p_L^* = p_R^*, \quad s_{xx,L}^* = s_{xx,R}^*. \tag{26}$$

From Eq.(26), we get that

$$\sigma_{x,L}^* = \sigma_{x,R}^*. \tag{27}$$

At last, for the λ_2 and λ_3 waves, one can find that the following two relations always hold:

$$u_L^* = u_R^*, \quad \sigma_{x,L}^* = \sigma_{x,R}^*. \tag{28}$$

For convenience, we define

$$s^* = u_L^* = u_R^*. \tag{29}$$

where s^* denotes the velocity of the contact wave.

3.4. A relation between ρ and s_{xx} in 1D elastic-plastic equation system

Thanks to (7), the equations of the density and the deviatoric stress in Eq.(11) can be written as

$$\frac{\partial u}{\partial x} = -\frac{1}{\rho}\frac{d\rho}{dt}, \tag{30}$$

and

$$\frac{ds_{xx}}{dt} = \frac{4}{3}\mu\frac{\partial u}{\partial x}. \tag{31}$$

Substituting (30) into (31) yields

$$\frac{ds_{xx}}{dt} = -\frac{4}{3}\mu\frac{1}{\rho}\frac{d\rho}{dt}. \tag{32}$$

Integrate the above equation from the data in front of a wave to the data behind the wave and perform some simple algebraic manipulations, one can get

$$s_{xx1} = -\frac{4}{3}\mu\ln(\frac{\rho_1}{\rho_0}) + s_{xx0}. \tag{33}$$

The subscripts 1 and 0 mean the states in front of and behind the wave, respectively. This relation always holds if there is no yielding in the integration path.

3.5. Building MHLLCEP

Now we consider the constructing details of MHLLCEP. There may be three to five waves existing in the Riemann structure, which depends on the yielding states on the left side and right side of the contact wave.

3.5.1. Pre-evaluating the states with a three-wave system

At first we do not know whether the states in the star region around the contact wave reach the elastic limit or not, so firstly *assume that there is only three waves and the material is totally yielding or totally not yielding* (**Assumption** 1). Based on **Assumption** 1, by using the HLLC Riemann solver, we can get the states in the star regions of the Riemann structure shown in Fig.1. If the

obtained state contains yielding process, we will consider the cases shown in Fig.2-4.

The Riemann structure of MHLLCEP shown in Fig.1 is given as follows,

$$\mathbf{U}_{Case1}^{\mathrm{MHLLCEP}}(x,t)=\begin{cases}\mathbf{U}_L, & \text{if} \quad \dfrac{x}{t}\le s_L,\\ \mathbf{U}_L^*, & \text{if} \quad s_L\le\dfrac{x}{t}\le s^*,\\ \mathbf{U}_R^*, & \text{if} \quad s^*\le\dfrac{x}{t}\le s_R,\\ \mathbf{U}_R, & \text{if} \quad \dfrac{x}{t}\ge s_R.\end{cases} \tag{34}$$

and the corresponding Eulerian numerical flux and Lagrangian numerical flux are

$$\mathbf{F}_{\mathrm{Case1}}^{\mathrm{Euler}}(x,t)=\begin{cases}\mathbf{F}_L, & \text{if} \quad \dfrac{x}{t}\le s_L,\\ \mathbf{F}_L^*, & \text{if} \quad s_L\le\dfrac{x}{t}\le s^*,\\ \mathbf{F}_R^*, & \text{if} \quad s^*\le\dfrac{x}{t}\le s_R,\\ \mathbf{F}_R, & \text{if} \quad \dfrac{x}{t}\ge s_R,\end{cases} \tag{35}$$

$$\mathbf{F}_{\mathrm{Case1}}^{\mathrm{Lag}}(x,t)=\begin{cases}\mathbf{f}_L^*, & \text{if} \quad s_*\ge\dfrac{x}{t},\\ \mathbf{f}_R^*, & \text{if} \quad s^*\le\dfrac{x}{t},\end{cases} \tag{36}$$

where $f=(0,p-s_{xx},(p-s_{xx})u)^T$.

According to the integrated Rankine-Hugoniot conditions of the left-going wave, one can get

$$\mathbf{F}_L^*=\mathbf{F}_L+s_L(\mathbf{U}_L^*-\mathbf{U}_L). \tag{37}$$

The first and second components of the above system can be written as

$$\rho_L^*u_L^*=\rho_Lu_L+s_L(\rho_L^*-\rho_L), \tag{38}$$

and

$$\rho_L^*u_R^{*2}-\sigma_L^*=\rho_Lu_L^2-\sigma_L+s_L(\rho_L^*u_L^*-\rho_Lu_L). \tag{39}$$

By using the relation of $u_L^*=u_R^*=s^*$ in Eq.(29), the speed of contact wave

can be evaluated as

$$\hat{s}^* = \frac{\sigma_L - \sigma_R + \rho_L u_L(s_L - u_L) - \rho_R u_R(s_R - u_R)}{\rho_L(s_L - u_L) - \rho_R(s_R - u_R)}, \tag{40}$$

the density is solved as

$$\hat{\rho}_L^* = \frac{\rho_L(u_L - s_L)}{\hat{s}^* - s_L}. \tag{41}$$

Similarly, the density behind the right going wave can be given as

$$\hat{\rho}_R^* = \frac{\rho_R(u_R - s_R)}{\hat{s}^* - s_R}. \tag{42}$$

Thanks to Eq.(33), the deviatoric stress is evaluated as

$$\hat{s}_{xxL}^* = -\frac{4}{3}\mu \ln(\frac{\hat{\rho}_L^*}{\rho_L}) + s_{xxL}, \quad \hat{s}_{xxR}^* = -\frac{4}{3}\mu \ln(\frac{\hat{\rho}_R^*}{\rho_R}) + s_{xxR}. \tag{43}$$

If the speeds of left- and right-going waves are given, we can evaluate all states in the star regions on the two sides of the contact wave. Here we define the speeds of left- and right-going waves as

$$s_L = \min(u_L - c_L, u_R - c_R, 0), \quad s_R = \max(u_L + c_L, u_R + c_R, 0). \tag{44}$$

By using the definition of wave speeds in (44), also in the following (71) and (93), s_L is strictly non-positive and s_R is strictly non-negative. For subsonic flows, the definition of the wave speeds is the same as the definition by Davis [20]; for supersonic flows, our definition will increase the numerical dissipation and is helpful for improving the stability of the scheme.

By using the pre-evaluated values of $\hat{s}_{xxL}^*$ and $\hat{s}_{xxR}^*$ in (43), we can classify the true condition into the following four cases.

3.5.2. Case 1: With only three waves

If ($|s_{xxL}| < \frac{2}{3}Y_0$, $|\hat{s}_{xxL}^*| < \frac{2}{3}Y_0$) and ($|s_{xxR}| < \frac{2}{3}Y_0$, $|\hat{s}_{xxR}^*| < \frac{2}{3}Y_0$), all the states are not yielding and there is no plastic wave. Similarly, if ($|s_{xxL}| \geq \frac{2}{3}Y_0$, $|\hat{s}_{xxL}^*| \geq \frac{2}{3}Y_0$) and ($|s_{xxR}| \geq \frac{2}{3}Y_0$, $|\hat{s}_{xxR}^*| \geq \frac{2}{3}Y_0$), all the states are yielding and

there is no elastic wave. In this case, the structures of the Riemann solver are shown in Fig.1, with only three waves.

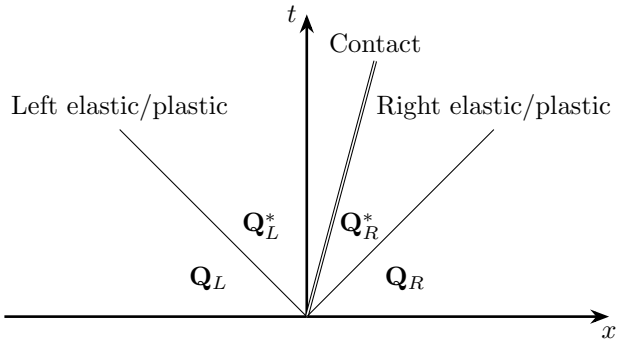

Figure 1: MHLLCEP approximate Riemann solver, case 1: with only plastic wave or elastic wave.

Then

$$s^* = \hat{s}^*, \quad \rho_L^* = \hat{\rho}_L^*, \quad \rho_R^* = \hat{\rho}_R^*, \tag{45}$$

$$s_{xxL}^* = \Upsilon(\hat{s}_{xxL}^*), \quad s_{xxR}^* = \Upsilon(\hat{s}_{xxR}^*), \tag{46}$$

where,

$$\Upsilon(\omega) = \begin{cases} \omega, \text{ if } |\omega| \leq \dfrac{2}{3}Y_0, \\ \dfrac{2}{3}Y_0, \text{ if } \omega > \dfrac{2}{3}Y_0, \\ -\dfrac{2}{3}Y_0, \text{ if } \omega < -\dfrac{2}{3}Y_0. \end{cases} \tag{47}$$

The Cauchy stresses are solved by Eq.(39),

$$\sigma_L^* = \sigma_R^* = \sigma_L - \rho_L(s_L - u_L)(s^* - u_L).$$

Then we can get the pressure:

$$p_L^* = s_{xxL}^* - \sigma_L^*, \; p_R^* = s_{xxR}^* - \sigma_R^*. \tag{48}$$

3.5.3. Case 2: with two waves in the left side and one wave in the right side of the contact wave

If $|s_{xxL}| \leq \frac{2}{3}Y_0 \leq |\hat{s}^*_{xxL}|$ and $|s_{xxR}| < \frac{2}{3}Y_0$, $|\hat{s}^*_{xxR}| < \frac{2}{3}Y_0$ there are both elastic wave and plastic wave in the left and only one elastic wave in the right-hand side of the contact. However, if $|s_{xxL}| \leq \frac{2}{3}Y_0 \leq |\hat{s}^*_{xxL}|$ and $|s_{xxR}| \geq \frac{2}{3}Y_0$ and $|\hat{s}^*_{xxR}| \geq \frac{2}{3}Y_0$, there are both plastic wave and elastic wave in the left-hand side and only a plastic wave exists in the right-hand side. We consider this two situations in one case. Correspondingly, the Riemann structure of this case is shown in Fig.2. We need to solve the yielding state of $\widetilde{\mathbf{Q}}_L$. The MHLLCEP is given as follows in this case,

$$\mathbf{U}^{\text{MHLLCEP}}_{\text{Case2}}(x,t) = \begin{cases} \mathbf{U}_L, & \text{if} \quad \dfrac{x}{t} \leq \widetilde{s}_L, \\ \widetilde{\mathbf{U}}_L, & \text{if} \quad \widetilde{s}_L \leq \dfrac{x}{t} \leq s_L, \\ \mathbf{U}^*_L, & \text{if} \quad s_L \leq \dfrac{x}{t} \leq s^*, \\ \mathbf{U}^*_R, & \text{if} \quad s^* \leq \dfrac{x}{t} \leq s_R, \\ \mathbf{U}_R, & \text{if} \quad \dfrac{x}{t} \geq s_R, \end{cases} \tag{49}$$

and the corresponding Eulerian and Lagrangian numerical fluxes are

$$\mathbf{F}^{\text{Euler}}_{\text{Case2}}(x,t) = \begin{cases} \mathbf{F}_L, & \text{if} \quad \dfrac{x}{t} \leq \widetilde{s}_L, \\ \widetilde{\mathbf{F}}_L, & \text{if} \quad \widetilde{s}_L \leq \dfrac{x}{t} \leq s_L, \\ \mathbf{F}^*_L, & \text{if} \quad s_L \leq \dfrac{x}{t} \leq s^*, \\ \mathbf{F}^*_R, & \text{if} \quad s^* \leq \dfrac{x}{t} \leq s_R, \\ \mathbf{F}_R, & \text{if} \quad \dfrac{x}{t} \geq s_R, \end{cases} \tag{50}$$

$$\mathbf{F}^{\text{Lag}}_{\text{Case2}}(x,t) = \begin{cases} \mathbf{f}^*_L, & \text{if} \quad s_* \geq \dfrac{x}{t}, \\ \mathbf{f}^*_R, & \text{if} \quad s^* \leq \dfrac{x}{t}. \end{cases} \tag{51}$$

According to the Rankine-Hugoniot relation for the left elastic wave, one

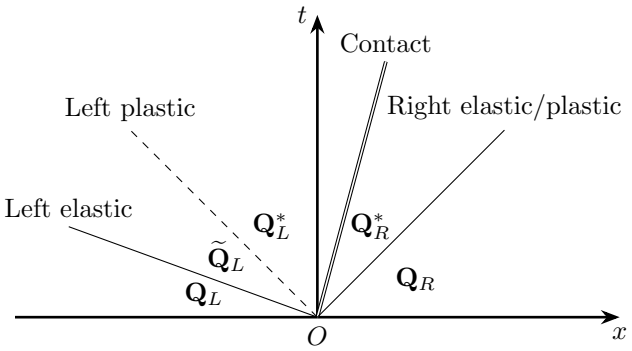

Figure 2: MHLLCEP approximate Riemann solver, case 2: with one wave in the right-hand side and two waves in the left-hand side.

can get

$$\widetilde{\rho}_L(\widetilde{u}_L - \widetilde{s}_L) = \rho_L(u_L - \widetilde{s}_L), \tag{52}$$

$$\widetilde{\rho}\widetilde{u}_L(\widetilde{u}_L - \widetilde{s}_L) = \rho_L u_L(u_L - \widetilde{s}_L) + \widetilde{\sigma}_L - \sigma_L, \tag{53}$$

$$\widetilde{\rho}\widetilde{E}_L(\widetilde{u}_L - \widetilde{s}_L) = \rho_L E_L(u_L - \widetilde{s}_L) + \widetilde{\sigma}_L\widetilde{u}_L - \sigma_L u_L, \tag{54}$$

where $\widetilde{s}_L$ denotes the speed of left elastic wave.

Because the deviatoric stress behind the elastic wave reaches the elastic limit, the deviatoric stress is taken as

$$\widetilde{s}_{xxL} = \begin{cases} -\dfrac{2}{3}Y_0, & \text{if} \quad \rho_L^* > \rho_L, \\ \dfrac{2}{3}Y_0, & \text{if} \quad \rho_L^* < \rho_L, \end{cases} \tag{55}$$

and thanks to Eq.(33), one can get

$$\widetilde{s}_{xxL} = \frac{4}{3}\mu \ln\frac{\widetilde{\rho}_L}{\rho_L} + s_{xxL}, \tag{56}$$

Thanks to the above two equations, the density behind the left elastic wave

can be given as

$$\widetilde{\rho}_L = \begin{cases} \rho_L \exp\left(\dfrac{Y_0}{2\mu} + \dfrac{3s_{xxL}}{4\mu}\right) & \text{if} \quad \rho_L^* > \rho_L, \\ \rho_L \exp\left(-\dfrac{Y_0}{2\mu} + \dfrac{3s_{xxL}}{4\mu}\right) & \text{if} \quad \rho_L^* < \rho_L. \end{cases} \tag{57}$$

The unknowns are the wave speed $\widetilde{s}_L$, the velocity $\widetilde{u}_L$, the pressure $\widetilde{p}_L$ and the specific internal energy $\widetilde{e}_L$. In the following, we will give the derivations of them.

Thanks to Eq.(52), one can get the wave speed

$$\widetilde{s}_L = \frac{\widetilde{\rho}_L \widetilde{u}_L - \rho_L u_L}{\widetilde{\rho}_L - \rho_L}. \tag{58}$$

Substituting Eq.(52) into Eq.(53) yields

$$\rho_L(\widetilde{u}_L - u_L)(u_L - \widetilde{s}_L) = \widetilde{\sigma}_L - \sigma_L. \tag{59}$$

Thanks to Eq.(52), one can get

$$u_L - \widetilde{s}_L = \frac{(u_L - \widetilde{u}_L)\widetilde{\rho}_L}{\widetilde{\rho}_L - \rho_L}. \tag{60}$$

Substituting Eq.(60) into (59) yields

$$-t(\widetilde{u}_L - u_L)^2 = \widetilde{\sigma}_L - \sigma_L, \tag{61}$$

where

$$t = \frac{\rho_L \widetilde{\rho}_L}{\widetilde{\rho}_L - \rho_L}. \tag{62}$$

Similar to Eq.(59), Eq.(53) can be changed into

$$t(u_L - \widetilde{u}_L)(\widetilde{E}_L - E_L) = \widetilde{\sigma}_L \widetilde{u}_L - \sigma_L u_L. \tag{63}$$

Because $E = e + \frac{1}{2}u^2$, one can get

$$\widetilde{e}_L - e_L = -\frac{\sigma_L + \widetilde{\sigma}_L}{2t}. \tag{64}$$

The EOS (5) can be written as

$$e = c_0 p - c_1 f(\rho/\rho_0), \tag{65}$$

where $c_0 = \frac{1}{\rho_0 \Gamma_0}$ and $c_1 = \frac{a_0^2}{\Gamma_0}$.

Substituting (65) and $\sigma = -p + s_{xx}$ into (64), we can get the pressure behind the elastic wave as

$$\widetilde{p}_L = \frac{2t(c_1 f(\widetilde{\rho}_L) + e_L) - (\sigma_L + \widetilde{s}_{xxL})}{2tc_0 - 1}, \tag{66}$$

and the Cauchy stress is solved by $\widetilde{\sigma}_L = -\widetilde{p}_L + \widetilde{s}_{xxL}$. By using Eq.(61) we can get

$$(\widetilde{u}_L - u_L)^2 = \frac{\sigma_L - \widetilde{\sigma}_L}{t}, \tag{67}$$

then the velocity is given as

$$\widetilde{\mathbf{u}}_L = \begin{cases} u_L + \sqrt{\dfrac{\sigma_L - \widetilde{\sigma}_L}{t}} & \text{if } \rho_R^* > \rho_R, \\ u_L - \sqrt{\dfrac{\sigma_L - \widetilde{\sigma}_L}{t}} & \text{if } \rho_R^* < \rho_R. \end{cases} \tag{68}$$

After solving the state of $\widetilde{\mathbf{Q}}_L$, using the similar process described in Section 3.5.2, the states of $\mathbf{Q}_L^*$ and $\mathbf{Q}_R^*$ can be solved out as follows.

The contact wave speed is

$$s^* = \frac{\widetilde{\sigma}_L - \sigma_R + \widetilde{\rho}_L \widetilde{u}_L (s_L - \widetilde{u}_L) - \rho_R u_R (s_R - u_R)}{\widetilde{\rho}_L (s_L - \widetilde{u}_L) - \rho_R (s_R - u_R)}, \tag{69}$$

The densities are

$$\rho_L^* = \frac{\widetilde{\rho}_L (\widetilde{u}_L - s_L)}{s^* - s_L}, \quad \rho_R^* = \frac{\rho_R (u_R - s_R)}{s^* - s_R}, \tag{70}$$

where the speed of the left plastic wave and right going wave are evaluated as

$$s_L = \min(\widetilde{u}_L - \widetilde{c}_L, u_R - c_R, 0), \quad s_R = \max(\widetilde{u}_L + \widetilde{c}_L, u_R + c_R, 0). \tag{71}$$

The deviatoric stresses are evaluated as

$$\overline{s}^*_{xxL} = \widetilde{s}_{xxL}, \;\; \overline{s}^*_{xxR} = -\frac{4}{3}\mu \ln(\frac{\rho^*_R}{\rho_R}) + s_{xxR}, \tag{72}$$

then using the von Mises' yielding condition:

$$s^*_{xxL} = \Upsilon(\overline{s}^*_{xxL}), \quad s^*_{xxR} = \Upsilon(\overline{s}^*_{xxR}). \tag{73}$$

The Cauchy stresses are given as

$$\sigma^*_L = \sigma^*_R = \widetilde{\sigma}_L - \widetilde{\rho}_L(s_L - \widetilde{u}_L)(s^* - \widetilde{u}_L), \tag{74}$$

and the pressures are

$$p^*_L = s^*_{xxL} - \sigma^*_L, \quad p^*_R = s^*_{xxR} - \sigma^*_R. \tag{75}$$

3.5.4. Case 3: with one wave in the left and two waves in the right of the contact wave

If $|s_{xxL}| < \frac{2}{3}Y_0$, $|\hat{s}^*_{xxL}| < \frac{2}{3}Y_0$ and $|s_{xxR}| \leq \frac{2}{3}Y_0 \leq |\hat{s}^*_{xxR}|$, there is only one elastic wave in the left and both elastic wave and plastic wave exist in the right-hand side. However, if $|s_{xxR}| \geq \frac{2}{3}Y_0$, $|\hat{s}^*_{xxR}| \geq \frac{2}{3}Y_0$ and $|s_{xxR}| \leq \frac{2}{3}Y_0 \leq |\hat{s}^*_{xxR}|$, there is only one plastic wave existing in the left and both the elastic and plastic wave exist in the right. Correspondingly, the Riemann structure of this case is shown in Fig.3. We need to solve the yielding state of $\widetilde{\mathbf{Q}}_R$. The MHLLCEP is given as follows in this case,

$$\mathbf{U}^{\mathrm{MHLLCEP}}_{\mathrm{Case3}}(x,t) = \begin{cases} \mathbf{U}_L, & \text{if} \quad \dfrac{x}{t} \le s_L, \\ \mathbf{U}^*_L, & \text{if} \quad s_L \le \dfrac{x}{t} \le s^*, \\ \mathbf{U}^*_R, & \text{if} \quad s^* \le \dfrac{x}{t} \le s_R, \\ \widetilde{\mathbf{U}}_R, & \text{if} \quad s_R \le \dfrac{x}{t} \le \widetilde{s}_R, \\ \mathbf{U}_R, & \text{if} \quad \dfrac{x}{t} \ge \widetilde{s}_R, \end{cases} \tag{76}$$

and the corresponding Eulerian and Lagrangian numerical flux are

$$\mathbf{F}^{\mathrm{Euler}}_{\mathrm{Case3}}(x,t) = \begin{cases} \mathbf{F}_L, & \text{if} \quad \dfrac{x}{t} \le s_L, \\ \mathbf{F}^*_L, & \text{if} \quad s_L \le \dfrac{x}{t} \le s^*, \\ \mathbf{F}^*_R, & \text{if} \quad s^* \le \dfrac{x}{t} \le s_R, \\ \widetilde{\mathbf{F}}_R, & \text{if} \quad s_R \le \dfrac{x}{t} \le \widetilde{s}_R, \\ \mathbf{F}_R, & \text{if} \quad \dfrac{x}{t} \ge \widetilde{s}_R, \end{cases} \tag{77}$$

$$\mathbf{F}^{\mathrm{Lag}}_{\mathrm{Case3}}(x,t) = \begin{cases} \mathbf{f}^*_L, & \text{if} \quad s_* \ge \dfrac{x}{t}, \\ \mathbf{f}^*_R, & \text{if} \quad s^* \le \dfrac{x}{t}. \end{cases} \tag{78}$$

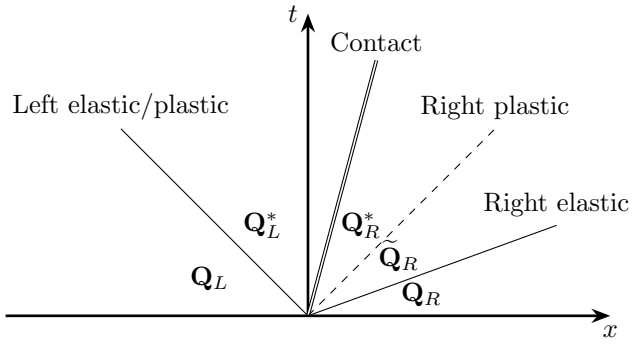

Figure 3: MHLLCEP approximate Riemann solver, case 3: with one wave in the left and two waves in the right.

The deviatoric stress, density and pressure behind the right elastic wave are

given as

$$\widetilde{s}_{xxR} = \begin{cases} -\frac{2}{3}Y_0, & \text{if} \quad \rho_R^* > \rho_R, \\ \frac{2}{3}Y_0, & \text{if} \quad \rho_R^* < \rho_R, \end{cases} \quad \widetilde{\rho}_R = \begin{cases} \rho_R \exp\left(\frac{Y_0}{2\mu} + \frac{3s_{xxR}}{4\mu}\right) & \text{if} \quad \rho_R^* > \rho_R, \\ \rho_R \exp\left(-\frac{Y_0}{2\mu} + \frac{3s_{xxR}}{4\mu}\right) & \text{if} \quad \rho_R^* < \rho_R, \end{cases} \tag{79}$$

$$\widetilde{p}_R = \frac{2t(c_1 f(\widetilde{\rho}_R) + e_R) - (\sigma_R + \widetilde{s}_{xxR})}{2tc_0 - 1}, \quad t = \frac{\rho_R \widetilde{\rho}_R}{\widetilde{\rho}_R - \rho_R}, \tag{80}$$

where $c_0 = \frac{1}{\rho_0 \Gamma_0}$ and $c_1 = \frac{a_0^2}{\Gamma_0}$. The Cauchy stress and velocity are

$$\widetilde{\sigma}_R = -\widetilde{p}_R + \widetilde{s}_{xxR}, \tag{81}$$

$$\widetilde{u}_R = \begin{cases} u_R + \sqrt{\frac{\sigma_R - \widetilde{\sigma}_R}{t}} & \text{if} \ \ \rho_R^* > \rho_R, \\ u_R - \sqrt{\frac{\sigma_R - \widetilde{\sigma}_R}{t}} & \text{if} \ \ \rho_R^* < \rho_R. \end{cases} \tag{82}$$

After obtaining the state of $\widetilde{\mathbf{Q}}_R$, we can evaluate the states of $\mathbf{Q}_L^*$ and $\mathbf{Q}_R^*$. The contact wave speed is

$$s^* = \frac{\sigma_L - \widetilde{\sigma}_R + \rho_L u_L(s_L - u_L) - \widetilde{\rho}_R \widetilde{u}_R(s_R - \widetilde{u}_R)}{\rho_L(s_L - u_L) - \widetilde{\rho}_R(s_R - \widetilde{u}_R)}. \tag{83}$$

The densities are

$$\rho_L^* = \frac{\rho_L(u_L - s_L)}{s^* - s_L}, \quad \rho_R^* = \frac{\widetilde{\rho}_R(\widetilde{u}_R - s_R)}{s^* - s_R}, \tag{84}$$

where the speeds of the left-going wave and the right-going plastic wave are

$$s_L = \min(u_L - c_L, \widetilde{u}_R - \widetilde{c}_R, 0), \quad s_R = \max(u_L + c_L, \widetilde{u}_R + \widetilde{c}_R, 0). \tag{85}$$

The deviatoric stresses are

$$\overline{s}_{xxL}^* = -\frac{4}{3}\mu \ln(\frac{\rho_L^*}{\rho_L}) + s_{xxL}, \ \ \overline{s}_{xxR}^* = \widetilde{s}_{xxR}, \tag{86}$$

$$s_{xxL}^* = \Upsilon(\overline{s}_{xxL}^*), \quad s_{xxR}^* = \Upsilon(\overline{s}_{xxR}^*). \tag{87}$$

The Cauchy stresses are

$$\sigma_L^* = \sigma_R^* = \sigma_L - \rho_L(s_L - u_L)(s^* - u_L), \tag{88}$$

and the pressures are

$$p_L^* = s_{xxL}^* - \sigma_L^*, \quad p_R^* = s_{xxR}^* - \sigma_R^*. \tag{89}$$

3.5.5. Case 4: with five waves

If $|s_{xxL}| \leq \frac{2}{3}Y_0 \leq |\hat{s}_{xxL}^*|$ and $|s_{xxR}| \leq \frac{2}{3}Y_0 \leq |\hat{s}_{xxR}^*|$. There are both elastic waves and plastic waves in left-hand side and right-hand side of the contact wave as shown in Fig.4. For this case, the MHLLCEP Riemann solver is given as

$$\mathbf{U}_{\text{Case4}}^{\text{MHLLCEP}}(x,t) = \begin{cases} \mathbf{U}_L, & \text{if} \quad \dfrac{x}{t} \leq s_L, \\ \mathbf{U}_L^*, & \text{if} \quad s_L \leq \dfrac{x}{t} \leq \widetilde{s}_L, \\ \widetilde{\mathbf{U}}_L, & \text{if} \quad \widetilde{s}_L \leq \dfrac{x}{t} \leq s^*, \\ \widetilde{\mathbf{U}}_R, & \text{if} \quad s^* \leq \dfrac{x}{t} \leq \widetilde{s}_R, \\ \mathbf{U}_R^*, & \text{if} \quad \widetilde{s}_R \leq \dfrac{x}{t} \leq s_R, \\ \mathbf{U}_R, & \text{if} \quad \dfrac{x}{t} \geq s_R, \end{cases} \tag{90}$$

and the corresponding Eulerian and Lagrangian numerical flux are

$$\mathbf{F}_{\text{Case4}}^{\text{Euler}}(x,t) = \begin{cases} \mathbf{F}_L, & \text{if} \quad \dfrac{x}{t} \leq s_L, \\ \mathbf{F}_L^*, & \text{if} \quad \widetilde{s}_L \leq \dfrac{x}{t} \leq s_L, \\ \widetilde{\mathbf{F}}_L, & \text{if} \quad s_L \leq \dfrac{x}{t} \leq s^*, \\ \widetilde{\mathbf{F}}_R, & \text{if} \quad s^* \leq \dfrac{x}{t} \leq s_R, \\ \mathbf{F}_R^*, & \text{if} \quad s_R \leq \dfrac{x}{t} \leq \widetilde{s}_R, \\ \mathbf{F}_R, & \text{if} \quad \dfrac{x}{t} \geq s_R, \end{cases} \tag{91}$$

$$\mathbf{F}^{\text{Lag}}_{\text{Case4}}(x,t) = \begin{cases} \widetilde{\mathbf{f}}_L, & \text{if} \quad s_* \geq \dfrac{x}{t}, \\ \widetilde{\mathbf{f}}_R, & \text{if} \quad s^* \leq \dfrac{x}{t}. \end{cases} \tag{92}$$

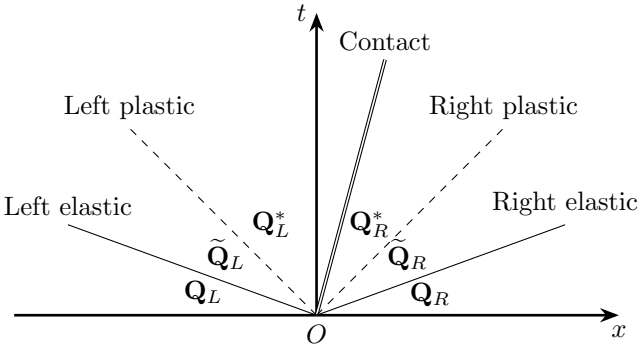

Figure 4: MHLLCEP approximate Riemann solver, case 4: with both left and right plastic waves.

The states of $\widetilde{\mathbf{Q}}_L$ and $\widetilde{\mathbf{Q}}_R$ can be evaluated by the same process given in Section 3.5.3 and Section 3.5.4. Then the states of $\mathbf{Q}_L^*$ and $\mathbf{Q}_R^*$ are given as following.

The speed of waves are evaluated as

$$s_L = \min(\widetilde{u}_L - \widetilde{c}_L, \widetilde{u}_R - \widetilde{c}_R, 0), \quad s_R = \max(\widetilde{u}_L + \widetilde{c}_L, \widetilde{u}_R + \widetilde{c}_R, 0), \tag{93}$$

$$s^* = \frac{\widetilde{\sigma}_L - \widetilde{\sigma}_R + \widetilde{\rho}_L \widetilde{u}_L (s_L - \widetilde{u}_L) - \widetilde{\rho}_R \widetilde{u}_R (s_R - \widetilde{u}_R)}{\widetilde{\rho}_L (s_L - \widetilde{u}_L) - \widetilde{\rho}_R (s_R - \widetilde{u}_R)}. \tag{94}$$

From Eq.(84), the densities behind the left and right elastic waves are given as

$$\rho_L^* = \frac{\widetilde{\rho}_L (\widetilde{u}_L - s_L)}{s^* - s_L}, \quad \rho_R^* = \frac{\widetilde{\rho}_R (\widetilde{u}_R - s_R)}{s^* - s_R}, \tag{95}$$

and the deviatoric stresses are given as

$$\overline{s}^*_{xxL} = \widetilde{s}_{xxL}, \tag{96}$$

$$\overline{s}^*_{xxR} = \widetilde{s}_{xxR}, \tag{97}$$

then using the von Mises' yielding condition

$$s^*_{xxL} = \Upsilon(\overline{s}^*_{xxL}), \quad s^*_{xxR} = \Upsilon(\overline{s}^*_{xxR}). \tag{98}$$

The Cauchy stresses are solved as

$$\sigma^*_L = \sigma^*_R = \widetilde{\sigma}_L - \widetilde{\rho_L}(s_L - \widetilde{u}_L)(s^* - \widetilde{u}_L). \tag{99}$$

Then we can get the pressure by $p = s_{xx} - \sigma$,

$$p^*_L = s^*_{xxL} - \sigma^*_L, \quad p^*_R = s^*_{xxR} - \sigma^*_R. \tag{100}$$

3.6. Summary of MHLLCEP

Here, we present all the procedures of MHLLCEP in a more simple way.

1. Assume that there are three waves in the Riemann solver. Based on this assumption, we perform the following evaluations:
   (a) evaluate $\hat{s}^*$

$$\hat{s}^* = \frac{\sigma_L - \sigma_R + \rho_L u_L(s_L - u_L) - \rho_R u_R(s_R - u_R)}{\rho_L(s_L - u_L) - \rho_R(s_R - u_R)}.$$

   (b) Evaluate $\hat{\rho}^*_L$ and $\hat{\rho}^*_R$

$$\hat{\rho}^*_L = \frac{\rho_L(u_L - s_L)}{s^* - s_L}, \quad \hat{\rho}^*_R = \frac{\rho_R(u_R - s_R)}{s^* - s_R}.$$

   (c) Evaluate the deviatoric stress

$$\hat{s}^*_{xxL} = -\frac{4}{3}\mu \ln(\frac{\hat{\rho}^*_L}{\rho_L}) + s_{xxL}, \;\; \hat{s}^*_{xxR} = -\frac{4}{3}\mu \ln(\frac{\hat{\rho}^*_R}{\rho_R}) + s_{xxR}.$$

   (d) Evaluate the pressure
2. Decide whether the state reaches the elastic limit or not
   (a) If $|s_{xxL}| < \frac{2}{3}Y_0 \leq |\hat{s}^*_{xxL}|$, two waves exist in the left, we need to evaluate the left yielding state.

The deviatoric stress, density and pressure behind the left elastic wave are given as

$$\widetilde{s}_{xxL} = \begin{cases} -\dfrac{2}{3}Y_0, & \text{if} \quad \rho_L^* > \rho_L, \\ \dfrac{2}{3}Y_0, & \text{if} \quad \rho_L^* < \rho_L, \end{cases}$$

$$\widetilde{\rho}_L = \begin{cases} \rho_L \exp\left(\dfrac{Y_0}{2\mu} + \dfrac{3s_{xxL}}{4\mu}\right) & \text{if} \quad \rho_L^* > \rho_L, \\ \rho_L \exp\left(-\dfrac{Y_0}{2\mu} + \dfrac{3s_{xxL}}{4\mu}\right) & \text{if} \quad \rho_L^* < \rho_L, \end{cases}$$

$$\widetilde{p}_L = \frac{2t(c_1 f(\widetilde{\rho}_L) + e_L) - (\sigma_L + \widetilde{s}_{xxL})}{2tc_0 - 1}, \quad t = \frac{\rho_L \widetilde{\rho}_L}{\widetilde{\rho}_L - \rho_L},$$

and the Cauchy stress and velocity are

$$\widetilde{\sigma}_L = -\widetilde{p}_L + \widetilde{s}_{xxL},$$

$$\widetilde{u}_L = \begin{cases} u_L - \sqrt{\dfrac{\sigma_L - \widetilde{\sigma}_L}{t}} & \text{if } \rho_L^* > \rho_L, \\ u_L + \sqrt{\dfrac{\sigma_L - \widetilde{\sigma}_L}{t}} & \text{if } \rho_L^* < \rho_L. \end{cases}$$

If not,

$$\widetilde{\mathbf{Q}}_L = \mathbf{Q}_L.$$

(b) If $|s_{xxR}| < \frac{2}{3}Y_0 \leq |\hat{s}_{xxR}^*|$, right elastic and plastic wave exist, we need to evaluate the right yielding state.

The deviatoric stress, density and pressure behind the right elastic wave are given as

$$\widetilde{s}_{xxR} = \begin{cases} -\dfrac{2}{3}Y_0, & \text{if} \quad \rho_R^* > \rho_R, \\ \dfrac{2}{3}Y_0, & \text{if} \quad \rho_R^* < \rho_R, \end{cases} \quad \widetilde{\rho}_R = \begin{cases} \rho_R \exp\left(\dfrac{Y_0}{2\mu} + \dfrac{3s_{xxR}}{4\mu}\right) & \text{if} \quad \rho_R^* > \rho_R, \\ \rho_R \exp\left(-\dfrac{Y_0}{2\mu} + \dfrac{3s_{xxR}}{4\mu}\right) & \text{if} \quad \rho_R^* < \rho_R, \end{cases}$$

$$\widetilde{p}_R = \frac{2t(c_1 f(\widetilde{\rho}_R) + e_R) - (\sigma_R + \widetilde{s}_{xxR})}{2tc_0 - 1}, \quad t = \frac{\rho_R \widetilde{\rho}_R}{\widetilde{\rho}_R - \rho_R},$$

and the Cauchy stress and velocity are

$$\widetilde{\sigma}_R = -\widetilde{p}_R + \widetilde{s}_{xxR},$$

$$\widetilde{u}_R = \begin{cases} u_R + \sqrt{\dfrac{\sigma_R - \widetilde{\sigma}_R}{t}} & \text{if } \rho_R^* > \rho_R, \\ u_R - \sqrt{\dfrac{\sigma_R - \widetilde{\sigma}_R}{t}} & \text{if } \rho_R^* < \rho_R. \end{cases}$$

If not,

$$\widetilde{\mathbf{Q}}_R = \mathbf{Q}_R.$$

3. Re-evaluate the states in the star regions on both sides of the contact wave

   (a) Evaluate the wave speeds:

$$s_L = \min(\widetilde{u}_L - \widetilde{c}_L, \widetilde{u}_R - \widetilde{c}_R, 0), \quad s_R = \max(\widetilde{u}_L + \widetilde{c}_L, \widetilde{u}_R + \widetilde{c}_R, 0),$$

$$s^* = \frac{\widetilde{\sigma}_L - \widetilde{\sigma}_R + \widetilde{\rho}_L \widetilde{u}_L (s_L - \widetilde{u}_L) - \widetilde{\rho}_R \widetilde{u}_R (s_R - \widetilde{u}_R)}{\widetilde{\rho}_L (s_L - \widetilde{u}_L) - \widetilde{\rho}_R (s_R - \widetilde{u}_R)}.$$

   (b) Evaluate the densities:

$$\rho_L^* = \frac{\widetilde{\rho}_L (\widetilde{u}_L - s_L)}{s^* - s_L}, \quad \rho_R^* = \frac{\widetilde{\rho}_R (\widetilde{u}_R - s_R)}{s^* - s_R},$$

   (c) Evaluate the deviatoric stresses:

$$\widetilde{s}_{xxL}^* = \begin{cases} \widetilde{s}_{xxL} & if\ |\hat{s}_{xxL}^*| \geq \frac{2}{3} Y_0 \\ -\frac{4}{3}\mu \ln\left(\frac{\rho_L^*}{\widetilde{\rho}_L}\right) + \widetilde{s}_{xxL} & otherwise \end{cases},$$

$$\widetilde{s}_{xxR}^* = \begin{cases} \widetilde{s}_{xxR} & if\ |\hat{s}_{xxR}^*| \geq \frac{2}{3} Y_0 \\ -\frac{4}{3}\mu \ln\left(\frac{\rho_R^*}{\widetilde{\rho}_R}\right) + \widetilde{s}_{xxR} & otherwise \end{cases},$$

   then using the von Mises' yielding condition

$$s_{xxL}^* = \Upsilon(\widetilde{s}_{xxL}^*), \quad s_{xxR}^* = \Upsilon(\widetilde{s}_{xxR}^*).$$

(d) Evaluate the Cauchy stresses:

$$\sigma_L^* = \sigma_R^* = \widetilde{\sigma}_L - \widetilde{\rho_L}(s_L - \widetilde{u}_L)(s^* - \widetilde{u}_L).$$

(e) The pressure is given by $p = s_{xx} - \sigma$.

4. A High-order cell-centered Lagrangian scheme for 1D conservative hydrodynamic equations with the Wilkins' model

Here, we consider the following governing equations with the Wilkins' model and the von Mises' yielding condition

$$\begin{cases} \partial_t \rho + \partial_x(\rho u) = 0, \\ \partial_t(\rho u) + \partial_x(\rho u^2 + p - s_{xx}) = 0, \\ \partial_t(\rho E) + \partial_x([\rho E + p - s_{xx}]u) = 0, \\ \partial_t s_{xx} + u\partial_x s_{xx} - \dfrac{4}{3}\partial_x u = 0, \\ |s_{xx}| \leq \dfrac{2}{3}Y_0. \end{cases} \tag{101}$$

For a Lagrangian scheme, the governing equations also include the equation for moving the coordinates at the vertex of the mesh,

$$\frac{dx(t)}{dt} = u(x,t). \tag{102}$$

The spatial domain is discretized into N cells $I_i = [x_{i-1/2}, x_{i+1/2}]$ of space sizes $\Delta x_i = x_{i+1/2} - x_{i-1/2}$ for $i = 1, 2, \cdots, N$. For a given cell I_i, the cell center is denoted by x_i. The velocity $u_{i+1/2}$ is defined at the vertex of the mesh. The value of the cell average for the cell I_i is defined by

$$\overline{\mathbf{Q}}_i = \frac{1}{\Delta x_i}\int_{I_i} \mathbf{Q} dx. \tag{103}$$

4.1. Spatial discretization

The semi-discrete finite volume scheme of the conservative equations (1) in the cell I_i is written as

$$\frac{d(\overline{\mathbf{U}}_i \Delta x_i)}{dt} = -(\mathbf{f}_{i+\frac{1}{2}} - \mathbf{f}_{i-\frac{1}{2}}), \tag{104}$$

where

$$\mathbf{f}_{i+\frac{1}{2}} = \mathbf{\Phi}(\mathbf{Q}_{L,i+\frac{1}{2}}, \mathbf{Q}_{R,i+\frac{1}{2}}) = \begin{bmatrix} 0 \\ p_{i+\frac{1}{2}} - (s_{xx})_{i+\frac{1}{2}} \\ (p_{i+\frac{1}{2}} - (s_{xx})_{i+\frac{1}{2}}) u_{i+\frac{1}{2}} \end{bmatrix}, \tag{105}$$

$\mathbf{Q}_{L,i+\frac{1}{2}}$ and $\mathbf{Q}_{R,i+\frac{1}{2}}$ represent the left and right values of $\mathbf{Q}$ at the cell's boundary $x_{i+\frac{1}{2}}$, respectively, and $p_{i+\frac{1}{2}}$, $(s_{xx})_{i+\frac{1}{2}}$ and $u_{i+\frac{1}{2}}$ denote the Godunov values of p, s_{xx} and u at $x_{i+\frac{1}{2}}$, respectively.

The Godunov values $\mathbf{Q}_{i+\frac{1}{2}}$ can be solved by the Riemann problem (11) at $x_{i+\frac{1}{2}}$,

$$\mathbf{Q}_{i+\frac{1}{2}} = \begin{cases} \mathbf{Q}_L^*, & \text{if} \quad \dfrac{dx}{dt} \le s^*, \\ \mathbf{Q}_R^*, & \text{if} \quad \dfrac{dx}{dt} > s^*, \end{cases} \tag{106}$$

where $\mathbf{Q}_L^*$, $\mathbf{Q}_R^*$ and s^* are evaluated by the MHLLCEP in Section 3.

Before this, we must give the left and right initial values ($\mathbf{Q}_{L,i+\frac{1}{2}}$ and $\mathbf{Q}_{R,i+\frac{1}{2}}$) of the Riemann problem in (11) by the cell average value $\overline{\mathbf{Q}}$ ($i = 1, 2, \cdots, N$). This process is done by the spatial reconstruction.

4.1.1. High-order reconstruction

The reconstruction is carried out in the characteristic variable space in this paper.

First, we transform the conservative variables to local characteristic variables,

$$\mathbf{W} = \mathbf{L} \cdot \overline{\mathbf{Q}}, \tag{107}$$

where $\mathbf{L}$ is the left eigenvector of $\mathbf{J}$, and $\mathbf{J}_i$ is the Jacobian matrix (13) in I_i.

Here, based on the cell average of $\mathbf{W}$, we first use the third-order modified WENO scheme constructed in Ref.([19]) to reconstruct the characteristic variables at the left and right interfaces ($\mathbf{W}_L$ and $\mathbf{W}_R$) of every cell and then project the reconstructed values of $\mathbf{W}$ back to the conservative variable space,

$$\mathbf{Q}_L = \mathbf{R} \cdot \mathbf{W}_L, \quad \mathbf{Q}_R = \mathbf{R} \cdot \mathbf{W}_R, \tag{108}$$

where $\mathbf{R}$ is the right eigenvector of $\mathbf{J}$.

4.1.2. Spatial discretization of the constitutive equation

In the Lagrangian frame, the equation of the constitute model (9) can be written as

$$\frac{ds_{xx}}{dt} = \frac{4\mu}{3}\frac{\partial u}{\partial x}, \tag{109}$$

In order to satisfy the geometrical conservation law, the volume of the cell I_i is evaluated by

$$V_i(t) = x_{i+\frac{1}{2}}(t) - x_{i-\frac{1}{2}}(t). \tag{110}$$

Taking the material derivative at both sides, we can get

$$\dot{V}_i(t) = \dot{x}_{i+\frac{1}{2}}(t) - \dot{x}_{i-\frac{1}{2}}(t). \tag{111}$$

Thanks to (102), the above equation can be written as

$$\dot{V}_i(t) = u_{i+\frac{1}{2}}(t) - u_{i-\frac{1}{2}}(t). \tag{112}$$

Combining (110), one can get

$$\frac{\dot{V}_i(t)}{V_i} = \frac{u_{i+\frac{1}{2}}(t) - u_{i-\frac{1}{2}}(t)}{x_{i+\frac{1}{2}}(t) - x_{i-\frac{1}{2}}(t)}, \tag{113}$$

By using Eq.(8), we can get

$$\frac{\partial u}{\partial x} = \frac{u_{i+\frac{1}{2}}(t) - u_{i-\frac{1}{2}}(t)}{x_{i+\frac{1}{2}}(t) - x_{i-\frac{1}{2}}(t)}. \tag{114}$$

Then the discretization of the constitutive equation is given as

$$\frac{ds_{xx}}{dt} = \frac{4\mu}{3}\frac{u_{i+\frac{1}{2}}(t) - u_{i-\frac{1}{2}}(t)}{x_{i+\frac{1}{2}}(t) - x_{i-\frac{1}{2}}(t)}. \tag{115}$$

4.1.3. High-order ghost-cell reconstruction method for Multi-material problems

For multi-material elastic-plastic flows, directly using the high-order reconstruction method introduced in Section 4.1.1 may result in numerical oscillations near the material interface. In order to delete these numerical oscillations, we develop a high-order ghost-cell reconstruction method which includes three procedures.

First step: track the interface by adding a marker function Mrk to mark the material in a cell. For two materials problem, the initial Mrk is defined as

$$\begin{cases} \text{Mrk}(i) = 0, & \text{if cell } i \text{ is of material A,} \\ \text{Mrk}(i) = 1, & \text{if cell } i \text{ is of material B.} \end{cases} \tag{116}$$

if $\text{Mrk}_{ii} = 0$ and $\text{Mrk}_{ii+1} = 1$, the interface is located at $x_{ii+\frac{1}{2}}$ between cell ii and $ii+1$;

Second step: if the reconstruction stencil is not across $x_{ii+\frac{1}{2}}$, we can directly use the high-order reconstruction method introduced in Section 4.1.1; if the stencil is across $x_{ii+\frac{1}{2}}$, we need define ghost cells. For example, we want to perform the third-order reconstruction on the left side of the interface and the reconstruction needs to use the stencil: $S^3 = (I_{ii-1}, I_{ii}, I_{ii+1})$. We can see that the cell I_{ii+1} is on the other side of the interface with a different EOS. Directly using the stencil S^3 to preform the reconstruction may result in numerical oscillations. Shown in Fig.5, we need to define a ghost cell I'_{ii+1} on the right side to replace the values on I_{ii+1}.

The cell average values of the ghost cell I'_{ii+1} is given as follows: the Cauchy stress and the velocity are continuous across the interface according to the re-

lations in Eq.(28), so we use the real values on the cell I_{ii+1} :

$$\overline{\sigma}'_{ii+1} = \overline{\sigma}_{ii+1}, \quad \overline{u}'_{ii+1} = \overline{u}_{ii+1}. \tag{117}$$

However, the values of pressure and density may be not continuous, so we use a reflected condition on the interface as

$$\overline{p}'_{ii+1} = \overline{p}_{ii}, \quad \overline{\rho}'_{ii+1} = \overline{\rho}_{ii}. \tag{118}$$

After we get all the primitive variables on the ghost cell I'_{ii+1}, using the EOS of material A on the left, we can get all the conservative variables $\mathbf{Q}'_{ii+1}$.

Third step: Define a new stencil $\widetilde{S}^3 = (I_{ii-1}, I_{ii}, I'_{ii+1})$. Based on the new stencil, the reconstruction on the left side of $x_{ii+\frac{1}{2}}$ can be given by using the high-order reconstruction method introduced in Section 4.1.1.

If we want to perform the reconstruction on the right side of $x_{ii+\frac{1}{2}}$, we use the similar process to do: define a new stencil $\widetilde{S}^3 = (I'_{ii}, I_{ii+1}, I_{ii+2})$, variables on the ghost cell I'_{ii} are defines as follows:

$$\overline{\sigma}'_{ii} = \overline{\sigma}_{ii}, \quad \overline{u}'_{ii} = \overline{u}_{ii}.$$

$$\overline{p}'_{ii} = \overline{p}_{ii-1}, \quad \overline{\rho}'_{ii} = \overline{\rho}_{ii+1}.$$

Other procedures are same as those for the reconstruction on the left side.

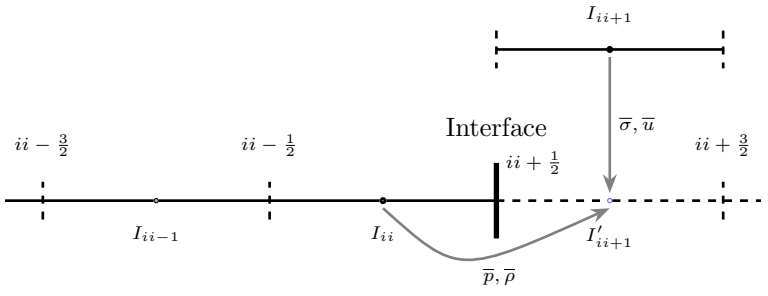

Figure 5: Ghost cell near the interface.

4.2. Time discretization

We use the third-order TVD-Runge-Kutta method [21] as the time marching method, the TVD-Runge-Kutta method used in the Lagrangian schemes with the von Mises' yielding condition is given in Ref.([1]) as follows.

Step 1,

$$\begin{aligned}
&x_{i+\frac{1}{2}}^{(1)} = x_{i+\frac{1}{2}}^{(0)} + \Delta t^n u_{i+\frac{1}{2}}^{(0)},\\
&\Delta x_i^{(1)} = x_{i+\frac{1}{2}}^{(1)} - x_{i-\frac{1}{2}}^{(1)},\\
&\Delta x_i^{(1)} \overline{\mathbf{U}}_i^{(1)} = \Delta x_i^{(0)} \overline{\mathbf{U}}_i^{(0)} + \Delta t^n \mathbf{L}(\overline{U}_i^{(0)}, (\overline{s_{xx}})_i^{(0)}, x_{i+\frac{1}{2}}^{(0)}),\\
&(\overline{\hat{s}_{xx}})_i^{(1)} = (\overline{s_{xx}})_i^{(0)} + \Delta t^n \Theta(u_{i+\frac{1}{2}}^{(0)}, x_{i+\frac{1}{2}}^{(0)}),\\
&(\overline{s_{xx}})_i^{(1)} = \Upsilon((\overline{\hat{s}_{xx}})_i^{(1)}).
\end{aligned} \tag{119}$$

Step 2,

$$\begin{aligned}
&x_{i+\frac{1}{2}}^{(2)} = \frac{3}{4} x_{i+\frac{1}{2}}^{(0)} + \frac{1}{4}\left(x_{i+\frac{1}{2}}^{(1)} + \Delta t^n u_{i+\frac{1}{2}}^{(1)}\right),\\
&\Delta x_i^{(2)} = x_{i+\frac{1}{2}}^{(2)} - x_{i-\frac{1}{2}}^{(2)},\\
&\Delta x_i^{(2)} \overline{\mathbf{U}}_i^{(2)} = \frac{3}{4}\Delta x_i^{(0)} \overline{\mathbf{U}}_i^{(0)} + \frac{1}{4}\left(\Delta x_i^{(1)} \overline{\mathbf{U}}_i^{(1)} + \Delta t^n \mathbf{L}(\overline{U}_i^{(1)}, (\overline{s_{xx}})_i^{(1)}, x_{i+\frac{1}{2}}^{(1)}\right),\\
&(\overline{\hat{s}_{xx}})_i^{(2)} = \frac{3}{4}(\overline{s_{xx}})_i^{(0)} + \frac{1}{4}\left((\overline{s_{xx}})_i^{(1)} + \Delta t^n \Theta(u_{i+\frac{1}{2}}^{(1)}, x_{i+\frac{1}{2}}^{(1)})\right),\\
&(\overline{s_{xx}})_i^{(2)} = \Upsilon((\overline{\hat{s}_{xx}})_i^{(2)}).
\end{aligned} \tag{120}$$

Step 3,

$$\begin{aligned}
&x_{i+\frac{1}{2}}^{(3)} = \frac{1}{3} x_{i+\frac{1}{2}}^{(0)} + \frac{2}{3}\left(x_{i+\frac{1}{2}}^{(2)} + \Delta t^n u_{i+\frac{1}{2}}^{(2)}\right),\\
&\Delta x_i^{(3)} = x_{i+\frac{1}{3}}^{(2)} - x_{i-\frac{1}{2}}^{(3)},\\
&\Delta x_i^{(3)} \overline{\mathbf{U}}_i^{(2)} = \frac{1}{3}\Delta x_i^{(0)} \overline{\mathbf{U}}_i^{(0)} + \frac{2}{3}\left(\Delta x_i^{(1)} \overline{\mathbf{U}}_i^{(2)} + \Delta t^n \mathbf{L}(\overline{U}_i^{(2)}, (\overline{s_{xx}})_i^{(2)}, x_{i+\frac{1}{2}}^{(2)}\right),\\
&(\overline{\hat{s}_{xx}})_i^{(3)} = \frac{1}{3}(\overline{s_{xx}})_i^{(0)} + \frac{2}{3}\left((\overline{s_{xx}})_i^{(2)} + \Delta t^n \Theta(u_{i+\frac{1}{2}}^{(2)}, x_{i+\frac{1}{2}}^{(2)})\right),\\
&(\overline{s_{xx}})_i^{(3)} = \Upsilon((\overline{\hat{s}_{xx}})_i^{(3)}).
\end{aligned} \tag{121}$$

Where $\mathbf{L}$ and Θ are the numerical spatial operators representing the right hands

of Eq.(104) and Eq.(115), respectively. The variables with the superscripts n and $n+1$ denote the values of the corresponding variables at the n-th and $(n+1)$-th time steps, respectively.

5. Numerical tests

In this section, our MHLLCEP Riemann solver is tested in different problems to see the capability of capturing elastic and plastic waves, especially in the problems with different materials. The third-order modified WENO scheme[19] with third-order TVD-Runge-Kutta method [21] is used, and the CFL is set as 0.5 in all the tests in the following.

5.1. Accuracy test

In the first test, a smooth solution is used to test the accuracy of the scheme. We consider the following compressible equations with source terms:

$$\begin{cases} \partial_t \rho + \partial_x(\rho u) = 0, \\ \partial_t(\rho u) + \partial_x(\rho u^2 + p - s_{xx}) = s_2, \\ \partial_t(\rho E) + \partial_x[(\rho E + p - s_{xx})u] = s_3, \\ \partial_t s_{xx} + u\partial_x s_{xx} - \dfrac{4}{3}\mu\partial_x u = 0, \end{cases} \tag{122}$$

where

$$s_2 = -2\pi\cos(2\pi(x-at))((ba_0^2 f_\eta(\eta) + s_0),$$

and $s_3 = as_2$.

The computational domain is $[0,1]$, and a periodic boundary condition is used. The EOS is given by the Mie-Grüneisen model with the parameters $\rho_0 = 8930\text{kg/m}^3$, $a_0 = 3940\text{m/s}$, $\Gamma_0 = 2$, and $s = 1.49$. The constitutive model has the following parameters, $\mu = 4.5 \times 10^{10}\text{Pa}$ and $Y^0 = 9 \times 10^{10}\text{Pa}$. The initial condition is given as

$$\rho = \rho_0(1 - b\sin(2\pi x)), \quad u = a, \quad s_{xx} = s_0\sin(2\pi x), \quad e = e_0, \tag{123}$$

where $a = 10,000\text{m/s}$, $b = 0.1$ and $s_0 = 6 \times 10^5\text{Pa}$, $e_0 = 0.1$.

The exact solution of above equations with the source terms are

$$\rho = \rho_0(1 - b\sin(2\pi(x - at))), \quad u = a, \quad s_{xx} = s_0\sin(2\pi(x - at)), \quad e = e_0. \tag{124}$$

The final results are given at time $t = 1$. The L_1- and L_∞-norm errors are shown in Table 1. We can see that, with a modified third-order WENO scheme, the high-order cell-centered Lagrangian scheme can approximately achieve the designed accuracy order.

Table 1: Errors for the smooth problem using the initially uniform mesh.

	N	L_1 error	L_1 order	L_∞ error	L_∞ order
ρ	50	5.45×10^{-4}	—	1.40×10^{-3}	—
	100	9.77×10^{-5}	2.48	4.47×10^{-4}	1.65
	200	1.43×10^{-5}	2.77	6.85×10^{-4}	2.71
	400	1.64×10^{-6}	3.12	1.07×10^{-5}	2.68
s_{xx}	50	3.55×10^{-5}	—	7.95×10^{-5}	—
	100	6.34×10^{-6}	2.48	2.48×10^{-5}	1.68
	200	9.10×10^{-7}	2.80	5.71×10^{-6}	2.12
	400	1.04×10^{-7}	3.13	8.92×10^{-7}	2.68

5.2. Piston problem

In the second test, we consider the piston problem [22] with a piece of copper with the initial condition of

$$\rho = 8930\text{kg/m}^3, \quad p = 10^5\text{Pa}, \quad u = 0\text{m/s}, \quad s_{xx} = 0\text{Pa}. \tag{125}$$

The EOS for copper is given by the Mie-Grüneisen model with the parameters

$$\rho_0 = 8930\text{kg/m}^3, \quad a_0 = 3940\text{m/s}, \quad ,\Gamma_0 = 2, \quad s = 1.49. \tag{126}$$

The constitutive model is characterized by the following parameters,

$$\mu = 4.5 \times 10^{10}\text{Pa}, \quad Y_0 = 9 \times 10^7\text{Pa}. \tag{127}$$

We use the velocity boundary condition with $u_{\text{piston}} = 20\text{m/s}$ on the left boundary and a wall boundary condition on the right boundary.

In Fig.6, we test the convergence of the scheme with different meshes of 100, 200 and 400 cells. The final time is $t = 150\mu s$. We can see that the current scheme can capture the leading elastic shock wave and the followed plastic wave well without numerical oscillations.

5.3. Wilkins' problem

This problem, first introduced by Wilkins[3], is used to test the ability of capturing rarefaction waves of a scheme. In this problem, a moving aluminium plate strikes on another aluminium plate. The EOS for aluminium is given by the Mie-Grüneisen model with the parameters $\rho_0 = 2785\text{kg/m}^3$, $a_0 = 5328\text{m/s}$, $\Gamma_0 = 2$ and $s = 1.338$. The constitutive model is characterized by the parameters $\mu = 2.76 \times 10^{10}\text{Pa}$ and $Y_0 = 3 \times 10^8\text{Pa}$. The initial condition is given as

$$\begin{cases} \rho = 2785\text{kg/m}^3, \quad u = 800\text{m/s}, \quad p = 10^{-6}\text{Pa}, \quad \text{if} \quad 0\text{m} \le x \le 0.005\text{m}, \\ \rho = 2785\text{kg/m}^3, \quad u = 0\text{m/s}, \quad p = 10^{-6}\text{Pa}, \quad \text{if} \quad 0.005\text{m} \le x \le 0.05\text{m}. \end{cases} \tag{128}$$

the left boundary is set as free boundary and on the right we use a wall boundary condition. The final time is $t = 5\times10^{-6}\text{s}$. In Fig.7, we give the results simulated with 200, 400 and 800 cells, the reference results are given by the refined mesh with 4000 cells. Shown in the figures and their locally enlarged plots, the elastic and plastic right-going shocks and the reflected elastic and plastic rarefaction waves are well resolved without numerical oscillations.

5.4. Multi-material problem 1

Here we consider the multi-material problem without plasticity effect. A similar case is used in Ref.([23]). In this test, a moving copper strikes on an aluminium plate. The parameters for the EOS and constitutive model for aluminum and copper are $(\rho_0, a_0, \Gamma_0, s, \mu)_{\text{Al}} = (8930\text{kg/m}^3, 3940\text{m/s}, 2, 1.49, 2.76, 2.76 \times 10^{10}\text{Pa})$ and $(\rho_0, a_0, \Gamma_0, s, \mu)_{\text{copper}} = (2785\text{kg/m}^3, 5328\text{m/s}, 2, 1.338, 4.5\times10^{10}\text{Pa})$,

ρ (kg/m^3)

u (m/s)

p (Pa)

s_{xx} (Pa)

Figure 6: The result of Piston problem

ρ (kg/m^3)

u (m/s)

p (Pa)

s_{xx} (Pa)

Figure 7: The result of Wilkins problem

respectively. In order to remove the influence of plasticity effect, we use a very large un-physical yielding strength $Y_0 = 3 \times 10^{12}$Pa. The initial condition of this problem is

$$\begin{cases} \rho = 2785\text{kg/m}^3, \ \ u = u_0, \ \ p = 10^{-12}\text{Pa}, s_{xx} = 0, \ \ \text{if } \ 0\text{m} \leq x \leq 0.025\text{m}, \\ \rho = 8930\text{kg/m}^3, \ \ u = 0\text{m/s}, \ \ p = 10^{-12}\text{Pa}, s_{xx} = 0, \ \ \text{if } \ 0.025\text{m} \leq x \leq 0.5\text{m}. \end{cases} \tag{129}$$

In this case we take $u_0 = 100$m/s. Figure 8 shows the numerical results computed by the scheme with HLLCE and the scheme with MHLLCEP at the final time $t = 2 \times 10^{-6}s$, the reference is given by a refined mesh with 4000 cells. We can see there is little difference between the two schemes for the multi-material case without plastic waves.

5.5. Two materials problem 2

Here we consider a similar problem as Section 5.4 but with plasticity effect. The yield strengths are $Y_0^{\text{Copper}} = 9 \times 10^7$ and $Y_0^{\text{Al}} = 3 \times 10^8$, respectively. All other parameters are same as those in problem 5.4. The initial condition is also as same as Eq.(129), we consider this case with a velocity of $u_0 = 60$m/s. Fig.9 gives the results at final time $t = 2 \times 10^{-6}$s with 400 cells, the solution computed by the scheme with HLLCE is taken as a comparison. The reference solution is given by the new scheme with 4000 cells. We can see that using HLLCE, because of the assumption that pressure is continuous across the contact wave, the Cauchy stress is not continuous across the interface, which is wrong obviously as it does not confirm with the relation of Eq.(28), while with MHLLCEP, there is no wrong obviously and numerical results are accordant with Eq.(28).

In this example, we also consider the effect of the ghost-cell method given in Section 4.1.3. Shown in Fig.10, without the use of ghost-cells, there are numerical oscillations existing near the interface, especially in the figures of pressure p and the derivative stress s_{xx}. The ghost-cell method can truly eliminate the numerical oscillations as analyzed.

ρ (kg/m^3)

u (m/s)

p (Pa)

σ_{xx} (Pa)

Figure 8: The result of two-materials problem 1

ρ (kg/m^3)

u (m/s)

p (Pa)

σ_{xx} (Pa)

Figure 9: The result of two-materials problem 2.

ρ (kg/m^3)

u (m/s)

p (Pa)

S_{xx} (Pa)

Figure 10: Comparison of the results with and without using of the ghost-cell method.

Conclusions

In this paper, the multi-material HLLC-type approximate Riemann solver with both the elastic and plastic waves (MHLLCEP) is constructed for 1D elastic-plastic flows with a hypo-elastic model and the von Mises yielding condition. During constructing the MHLLCEP, we do not use the assumption in which the pressure is continuous across the contact wave and so describing and evaluating the plastic waves are more accurate than that in the HLLCE. Based on the MHLLCEP, combining with the third-order ghost-cell reconstruction method and the third-order TVD-Runge-Kutta method in time, a high-order cell-centered Lagrangian scheme for 1D multi-material elastic flows is built. Verified by the numerical experiments, both the plastic waves and elastic waves can be resolved correctly, our third-order scheme appears to be convergent, stable, essentially non-oscillatory. Especially for multi-material elastic-plastic flows, the results solved by the scheme with HLLCE may result in wrong solutions, but our new scheme can eliminate these errors and leads to the reasonable numerical results. $(\rho_0, a_0, \Gamma_0, s, \mu)_{\mathrm{Al}} = (8930\mathrm{kg/m^3}, 3940\mathrm{m/s}, 2, 1.49, 2.76, 9 \times 10^7\mathrm{Pa})$
$(\rho_0, a_0, \Gamma_0, s, \mu)_{\mathrm{copper}} = (2785\mathrm{kg/m^3}, 5328\mathrm{m/s}, 2, 1.338, 3 \times 10^8\mathrm{Pa})$,
$\frac{4}{3}\mu > |\frac{\rho_0}{\rho}\Gamma_0 s_{xx}|$

Acknowledgement

This work was supported by NSFC(Grant No. 11672047) and Science Challenge Project (Grant No. TZ2016002).

References

[1] J. Cheng, Harten-Lax-van Leer-contact (HLLC) approximation Riemann solver with elastic waves for one-dimensional elastic-plastic problems, Applied Mathematics and Mechanics 37 (11) (2016) 1517–1538.

[2] E. F. Toro, M. Spruce, W. Speares, Restoration of the contact surface in the hll-riemann solver, Shock waves 4 (1) (1994) 25–34.

[3] M. L. Wilkins, Calculation of elastic-plastic flow, Tech. rep., California Univ Livermore Radiation Lab (1963).

[4] J. A. Trangenstein, P. Colella, A higher-order Godunov method for modeling finite deformation in elastic-plastic solids, Communications on Pure and Applied mathematics 44 (1) (1991) 41–100.

[5] G. Miller, P. Colella, A high-order Eulerian Godunov method for elastic–plastic flow in solids, Journal of computational physics 167 (1) (2001) 131–176.

[6] P. T. Barton, D. Drikakis, E. Romenski, V. A. Titarev, Exact and approximate solutions of Riemann problems in non-linear elasticity, Journal of Computational Physics 228 (18) (2009) 7046–7068.

[7] T. Liu, W. Xie, B. Khoo, The modified ghost fluid method for coupling of fluid and structure constituted with hydro-elasto-plastic equation of state, SIAM Journal on Scientific Computing 30 (3) (2008) 1105–1130.

[8] D. Burton, T. Carney, N. Morgan, S. Sambasivan, M. Shashkov, A cell-centered Lagrangian Godunov-like method for solid dynamics, Computers & Fluids 83 (2013) 33–47.

[9] G. Kluth, B. Després, Discretization of hyperelasticity on unstructured mesh with a cell-centered Lagrangian scheme, Journal of Computational Physics 229 (24) (2010) 9092–9118.

[10] P.-H. Maire, R. Abgrall, J. Breil, R. LoubèRe, B. Rebourcet, A nominally second-order cell-centered Lagrangian scheme for simulating elastic–plastic flows on two-dimensional unstructured grids, Journal of Computational Physics 235 (2013) 626–665.

[11] J.-B. Cheng, W. Huang, S. Jiang, B. Tian, A third-order moving mesh cell-centered scheme for one-dimensional elastic-plastic flows, Journal of Computational Physics 349 (2017) 137–153.

[12] S. L. Gavrilyuk, N. Favrie, R. Saurel, Modelling wave dynamics of compressible elastic materials, Journal of computational physics 227 (5) (2008) 2941–2969.

[13] B. Despres, A geometrical approach to nonconservative shocks and elasto-plastic shocks, Archive for Rational Mechanics and Analysis 186 (2) (2007) 275–308.

[14] J.-B. Cheng, E. F. Toro, S. Jiang, M. Yu, W. Tang, A high-order cell-centered Lagrangian scheme for one-dimensional elastic–plastic problems, Computers & Fluids 122 (2015) 136–152.

[15] E. F. Toro, Riemann solvers and numerical methods for fluid dynamics: a practical introduction, Springer Science & Business Media, 2013.

[16] G.-S. Jiang, C.-W. Shu, Efficient implementation of weighted ENO schemes, Journal of computational physics 126 (1) (1996) 202–228.

[17] C.-S. Huang, T. Arbogast, J. Qiu, An Eulerian–Lagrangian WENO finite volume scheme for advection problems, Journal of Computational Physics 231 (11) (2012) 4028–4052.

[18] M. Dumbser, W. Boscheri, High-order unstructured Lagrangian one-step WENO finite volume schemes for non-conservative hyperbolic systems: applications to compressible multi-phase flows, Computers & Fluids 86 (2013) 405–432.

[19] S. Liu, Y. Shen, B. Chen, F. Zeng, Novel local smoothness indicators for improving the third-order WENO scheme, International Journal for Numerical Methods in Fluids 87 (2) (2018) 51–69.

[20] S. Davis, Simplified second-order Godunov-type methods, SIAM Journal on Scientific and Statistical Computing 9 (3) (1988) 445–473.

[21] C.-W. Shu, S. Osher, Efficient implementation of essentially non-oscillatory shock-capturing schemes, Journal of computational physics 77 (2) (1988) 439–471.

[22] P.-H. Maire, R. Abgrall, J. Breil, J. Ovadia, A cell-centered Lagrangian scheme for two-dimensional compressible flow problems, SIAM Journal on Scientific Computing 29 (4) (2007) 1781–1824.

[23] N. S. Ghaisas, A. Subramaniam, S. K. Lele, High-order Eulerian methods for elastic-plastic flow in solids and coupling with fluid flows, in: 46th AIAA Fluid Dynamics Conference, 2016, p. 3350.